REVIEW ARTICLE

PECVD growth of carbon nanotubes: From experiment to simulation

Erik C. Neyts[a)]
Research Group PLASMANT, Dept. of Chemistry, University of Antwerp, Universiteitsplein 1, 2610 Wilrijk-Antwerp, Belgium

(Received 6 February 2012; accepted 22 March 2012; published 16 April 2012)

Nanostructured carbon materials show a tremendous variety in atomic structure, morphology, properties, and applications. As all properties are ultimately determined by the structure of the material, a thorough understanding of the growth mechanisms that give rise to the particular structure is critical. On many occasions, it has been shown that plasma enhanced growth can be strongly beneficial. This review will describe the authors' current understanding of plasma enhanced growth of carbon nanotubes, the prototypical example of nanostructured carbon materials, as obtained from experiments, simulations, and modeling. Specific emphasis is put on where experiments and computational approaches correspond, and where they differ. Also, the current status on simulating PECVD growth of some other carbon nanomaterials is reviewed, including amorphous carbon, graphene, and metallofullerenes. Finally, computational challenges with respect to the simulation of PECVD growth are identified. © *2012 American Vacuum Society*. [http://dx.doi.org/10.1116/1.3702806]

I. INTRODUCTION

Low temperature plasmas are a widespread and extremely versatile tool for material processing, including applications such as thin film deposition, etching, surface activation and functionalization, plasma polymerization, cleaning, ashing, surface hardening, oxidation, and so forth.[1,2] Especially in the microelectronics industry, plasmas have become indispensable for deposition and etching processes, due to their operation at low temperature. This low temperature operation is possible thanks to the activation of the gas by the energetic electrons, while the gas itself remains at temperatures at or slightly above room temperature.[3] Indeed, in a low temperature plasma, the electrons cause, among others, ionization, excitation, and dissociation. The dissociation reactions lead to the formation of highly reactive radicals. The ionization process creates ions and electrons that are accelerated by the applied electric field. These ions and electrons can subsequently participate in various reactions, including dissociation reactions, leading to the formation of more radicals. Finally, also the excited atoms and molecules, which are generally more reactive than the ground-state species, contribute to the enhanced reactivity of the processing gas, thereby omitting the need for high temperatures to achieve chemical reactions. As a result, the plasma contains numerous species affecting the deposition process, as depicted in Fig. 1: energetic ions, which may sputter material and heat the substrate; electrons, which cause chemical reactions to take place; photons, which also heat the substrate and possibly induce photochemical reactions; highly reactive radicals, which may deposit on the substrate or etch material; and a fraction of the undissociated source gas, which may also deposit and react at the substrate.[4] Also other factors, such as the electromagnetic fields in the plasma, may affect the deposition process, e.g., by promoting the vertical alignment of single walled carbon nanotubes (SWNTs).[5,6] In contrast, traditional thermal chemical vapor deposition (CVD) typically requires processing temperatures in the order of 1000 K or higher, in order to achieve the required energy for the chemical reactions to take place.[3] As we will see, this reactive plasma environment has several advantages over thermal growth when it comes to the growth of carbon nanotubes.

The organization of this review is as follows. In Sec. II, the various plasma sources used for the growth of carbon nanotubes (CNTs) are briefly discussed. Section III describes the CNTs in terms of their structure, properties, and applications. The various growth mechanisms as proposed throughout the years will be reviewed in Sec. IV, concentrating on SWNTs, as this is the subject of most simulation efforts. Also in Sec. IV, we shift our attention to plasma enhanced chemical vapor deposition (PECVD) growth of carbon nanotubes, with specific emphasis on the advantages of PECVD over thermal CVD growth. In Sec. V, we concentrate on the various modeling and simulation efforts with respect to CNTs, first describing *ab initio* simulations, followed by classical molecular dynamics simulations, and the more macroscale mechanistic models. Special attention will be paid to the comparison between these theoretical descriptions and experimental observations, and especially to what extent these different modeling and simulation approaches are approximations to the real growth process. Section VI gives a brief overview of modeling results for other nanostructured carbon materials, such as graphene, amorphous

[a)]Electronic mail: erik.neyts@ua.ac.be

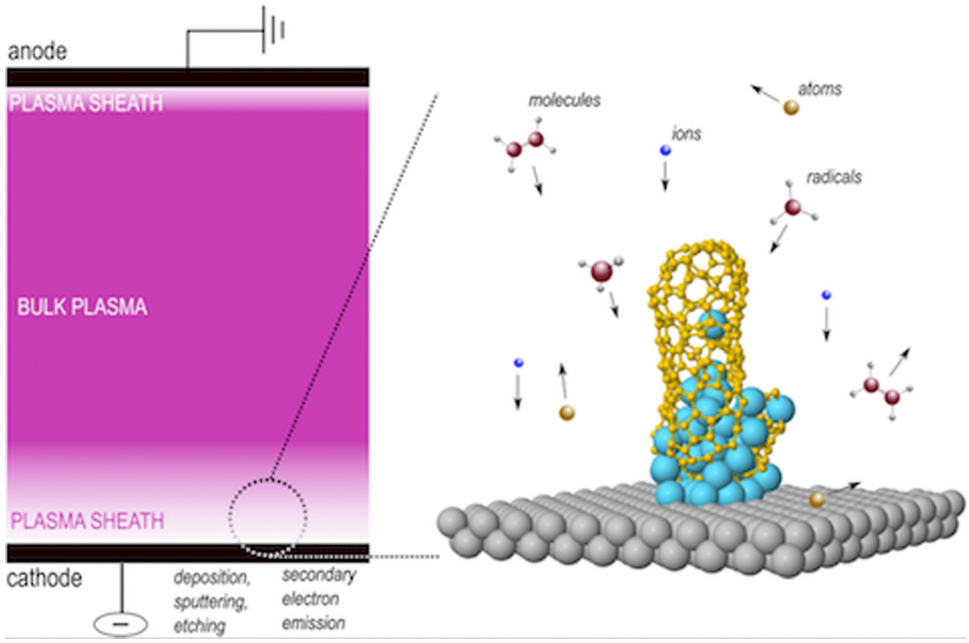

FIG. 1. (Color online) Typical dc plasma and its main constituents contributing to plasma surface interactions and specifically to CNT growth.

carbon, and metallofullerenes. Finally, Sec. VII is dedicated to future challenges regarding the modeling and simulation.

II. PECVD SOURCES FOR CNT GROWTH

Various plasma deposition reactors have been developed through the years. As far as CNT growth is concerned, one of the most widely used research sources is the direct current (dc) source. A schematic representation is shown in Fig. 2. It operates by applying a voltage across two (typically parallel) electrodes, causing gas breakdown. The created ions are accelerated toward the cathode, creating new electrons, thereby sustaining the plasma. Note that the potential drops very quickly over a short distance in front of the cathode, which is termed "the sheath." The pressure is typically in the order of a few Torr, while the voltage is typically several hundred volts. The substrate temperature can be controlled by either cooling or heating elements; often, however, the real growth temperature will deviate from the controlled substrate temperature due to plasma heating effects. Numerous interesting growth results have been obtained using this source, albeit various disadvantages render it less useful for commercial applications. Indeed, the substrate bias cannot be controlled independently from the applied voltage. Second, the required high voltages cause energetic ion bombardment, leading to damage or even erosion of the deposited material. Third, the electrodes need to be conducting to sustain the plasma.[1]

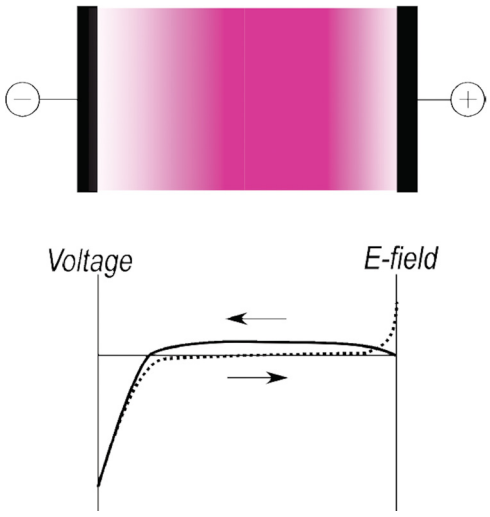

FIG. 2. (Color online) Typical dc plasma and its potential and electric field distribution.

One solution is the use of a capacitively coupled radio frequency (cc rf) source, in which one of the electrodes is coupled to an rf (e.g., 13.56 MHz) power supply.[7] This configuration leads to an alternating voltage between the two electrodes, preventing charges from building up at the electrodes, allowing the use of nonconductive electrodes, or the deposition of insulating material. In the cc rf source, the electrons can follow the instantaneous electric field, while the much heavier ions can typically only follow the time-averaged field. One important aspect of cc rf discharges is the development of a self-bias on the electrodes, which is inversely proportional to the square of the electrode area. Because of this self-bias, positive ions are continuously accelerated toward the powered electrode. The cc rf discharge operates at lower pressures than the dc source, typically in the order of a few hundred mTorr.

Another plasma source widely used for CNT growth is the inductively coupled plasma source (ICP).[8–11] In contrast to the dc and cc rf discharge, the ICP is a so-called electrodeless source, in which the rf power is coupled inductively through an induction coil, placed outside the reaction chamber, to the plasma. One important advantage is that contamination by the electrodes is avoided. Also, a much higher plasma density can be obtained in ICPs. While the plasma is created by means of the inductively coupled power, the

substrate can be biased independently by an additional dc or rf power supply. Hence, the sputtering ability of the ions can be controlled through the accelerating voltage across the sheath in front of the substrate.

Yet another plasma source used for CNT growth is microwave plasma chemical vapor deposition.[12–17] The microwave plasma is also a high density source, typically powered by 2.45 GHz. Again, the substrate voltage can be independently controlled using a dc or rf power supply. Here, too, the ion sputtering ability can be controlled by varying the substrate voltage.

Sources in which the plasma generation chamber is separated from the deposition chamber or, more generally, in which the plasma is not in direct contact with the substrate, are called remote plasmas. The advantage of using a remote plasma is that ion bombardment can be avoided. One example is the ICP source depicted in Fig. 3. In this particular example, the plasma is generated by an rf coil, generating plasma powers in the range 15–450 W. The actual substrate is located downstream from the plasma generation area. Hence, the generated radicals can reach the substrate by convection and diffusion, while in absence of an electric field at the substrate there is no ion bombardment. The substrate was heated by halogen lamps, and no temperature increase was detected due to the remote plasma. Using this source, SWNTs were successfully grown at temperatures as low as 673 K.[18]

All of the above-mentioned sources operate at subatmospheric pressures. However, operation at atmospheric pressure may be advantageous as no (expensive) vacuum pumps need to be installed. Furthermore, discharges operating at atmospheric pressure also have the advantage of suffering less from energetic ion bombardment: due to the higher pressure, the ions frequently collide, thereby losing most of their energy. This, in turn, results in less damage experienced by the growing tubes in an atmospheric pressure plasma enhanced chemical vapor deposition setup. Examples of CNT deposition at atmospheric pressure are the atmospheric pressure radio frequency discharge (see, e.g., Ref. 19, and references therein), and the dielectric barrier discharge (see, e.g., Ref. 20, and references therein).

III. STRUCTURE, PROPERTIES, AND APPLICATIONS OF CARBON NANOTUBES

A. Structure

Carbon nanotubes are hollow cylindrical structures composed of a hexagonal carbon network, first recognized by Iijima in 1991.[21] Conceptually, they may be thought of as rolled up graphene layers. When multiple concentric cylinders constitute the CNT, they are termed multiwalled carbon nanotubes (MWNTs). In MWNTs, the walls of each cylinder are parallel to the central axis. When the walls of the cylinders are tilted, the structure is termed carbon nanofiber (CNF). CNFs can adopt various structures, such as a stacked cone arrangement or a bamboolike structure. When only a single cylinder constitutes the CNT, it is termed a single walled carbon nanotube (SWNT).[20,22–24] Of special importance is how the graphene layer is rolled up. Since the circumference of the SWNT is given by a chiral vector $\mathbf{C}_h = n\mathbf{a}_1 + m\mathbf{a}_2$, where n and m are integers and $\mathbf{a}_1$ and $\mathbf{a}_2$ are the unit vectors of the hexagonal network, various SWNT structures can be formed for the same circumference but with different helicity. The (n,m) pair is termed the chirality of the SWNT. If $n = m$, the SWNT has the armchair structure. If $m = 0$, the SWNT is called zigzag. The angle between $\mathbf{C}$ and the zigzag line is the chiral angle. Thus, zigzag SWNTs have a chiral angle $\varphi = 0°$, while armchair SWNTs have a chiral angle $\varphi = 30°$. In all other cases, the SWNT is simply called "chiral." The structure of SWNTs is shown in Fig. 4. The chirality of the SWNT is of the utmost importance, as it determines the electronic properties of the SWNT. If $(n-m)$ is a multiple of 3, the SWNT is metallic; otherwise, it is semiconducting. Hence, all armchair SWNTs are metallic. A set of random n and m values therefore makes up a collection of SWNTs of which typically-one third is metallic, while two-thirds would be semiconducting.[25]

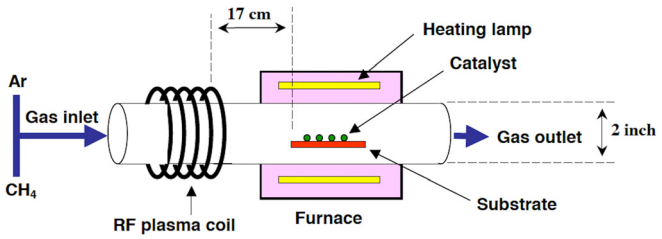

FIG. 3. (Color online) Remote PECVD source for CNT growth. Reprinted with permission from Bae *et al.*, Chem. Mater. **17**, 5141 (2005), American Chemical Society.

B. Properties and applications

Carbon nanotubes have truly amazing properties. Mechanically, their strength is a result of the strong sp^2–sp^2 bonds that make up the hexagonal network. Their Young's modulus can be as high as 1000 GPa, making them 5 times stronger than steel.[26] Their tensile strength can be as high as 150 GPa, i.e., about 100 times higher than that of steel and about 40 times higher than that of Kevlar®.[27] Their bulk modulus can exceed that of diamond, with measured values up to 546 GPa.[28] These mechanical properties allow CNTs

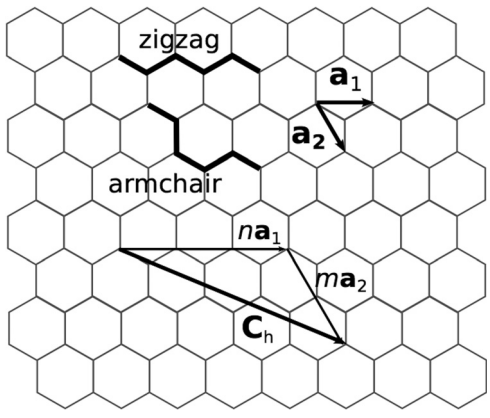

FIG. 4. Illustration of the determination of chirality of an SWNT, as dictated by the chiral vector $\mathbf{C}_h$. $\mathbf{a}_1$ and $\mathbf{a}_2$ are the primitive lattice vectors of the graphene sheet, and n and m are the characteristic integers, uniquely identifying the SWNT chirality.

to be used, e.g., as components in super-strong polymeric composite materials.

Electrically, metallic SWNTs can carry an electric current density of 4×10^9 A/cm^2, which is 1000 times higher than that of copper,[29] offering perspective for their use as interconnects in silicon IC fabrication.

Optically, CNT forests show absorbances up to 0.99, thereby forming a nearly ideal blackbody in the range 200–200 μm.[30] Finally, CNTs are also very good thermal conductors, showing a room temperature thermal conductivity of about 3500 W m^{-1} K^{-1},[31] allowing them to be used as heat sinks in order to dissipate heat from computer chips.

In particular, SWNTs offer perspective in electronic applications, since they can be either metallic or semiconducting, with a bandgap ranging from 0 eV to about 1 eV, depending on their chirality and diameter. They allow one-dimensional conduction and are envisaged for use in nanoscale electronics such as single electron transistors, as electron field emitters, for hydrogen storage, as actuators, chemical sensors, etc.[32] Furthermore, many properties of SWNTs are tunable to the required application, such as their photoelectrochemical activity by controlling their length. This offers opportunities in, e.g., fabrication of efficient optoelectronic devices, nanotube optical detectors, or emitters.[33]

Whereas CNTs are already effectively used in, e.g., mechanical applications, most electronic applications cannot yet be realized, due to our current inability to control the growth of CNTs exactly, especially regarding the required electronic properties.

IV. CNT GROWTH

Various methods exist for growing carbon nanotubes, including electric arc discharges, laser ablation, fullerene recrystallization, catalyzed chemical vapor deposition (CCVD), and PECVD. In the following, the most important growth mechanisms are summarized, focusing on the mechanisms for CCVD and PECVD.

A. CNT growth mechanisms

While not developed for CCVD growth, one of the earliest mechanisms proposed for CNT growth is the so-called "scooter mechanism," first proposed by the Smalley group.[34] In this model, devised for arc growth and laser ablation growth, one or a few atoms of the metal catalyst are envisioned to be attached to the growing carbon tube, circulating/scooting around the perimeter of the open end of the tube. These atoms then allow the incorporation of new carbon atoms to the tubular structure, while preventing closure of the tube. This model, however, has been abandoned based on more recent *ab initio* calculations. For example, Charlier *et al.* demonstrated how a single cobalt atom is incorporated in the tip of the tube instead of scooting around the open edge, allowing for a closed-end growth mechanism.[35]

One widely accepted mechanism is the vapor–liquid–solid mechanism (VLS), which was adopted from the growth of silicon whiskers.[36] This model was then adapted for tubular carbon growth by Baker *et al.*[37] An illustration of this model is shown in Fig. 5. In this mechanism, hydrocarbon molecules from the vapor phase adsorb on the liquid metal nanoparticle. The particle catalytically decomposes the hydrocarbon molecule in single carbon atoms, which dissolve in the liquid particle. After supersaturation of the particle, a solid network must form by surface segregation from the cluster, subsequently resulting in the formation of the solid CNT.

A variant of this mechanism was suggested by Page *et al.* These authors proposed a vapor–solid–solid model[38] for explaining the growth of SWNTs on nontraditional catalysts such as SiO_2. In this mechanism, CO is formed, resulting in the reduction of the SiO_2 surface with the formation of a solid SiC shell surrounding the solid SiO_2 particle. Subsequently, the continued addition of carbon to the surface leads to the formation of the CNT.

Furthermore, whereas thermal CVD growth of CNTs typically operates at temperatures above about 700 K, PECVD may operate at lower temperatures, opening up the possibility of growing CNTs on solid particles instead of on liquid particles. Hofmann *et al.* have proposed a surface-mediated growth model explaining the lower activation energy associated with PECVD growth.[39,40] In this model, carbon transport is not by bulk diffusion through the liquid particle, but rather by surface diffusion over a possibly solid particle. This was evidenced by the measured activation barrier of 0.23 eV on a nickel catalyst, which is indeed markedly lower than the typical activation energy of 1.2 eV in thermal growth.[40]

Finally, an entirely different model was proposed recently by Ding *et al.*, i.e., the so-called screw-dislocation model.[41] In this model, the growth rate is shown to be proportional to the chiral angle, due to the presence of a screw dislocation

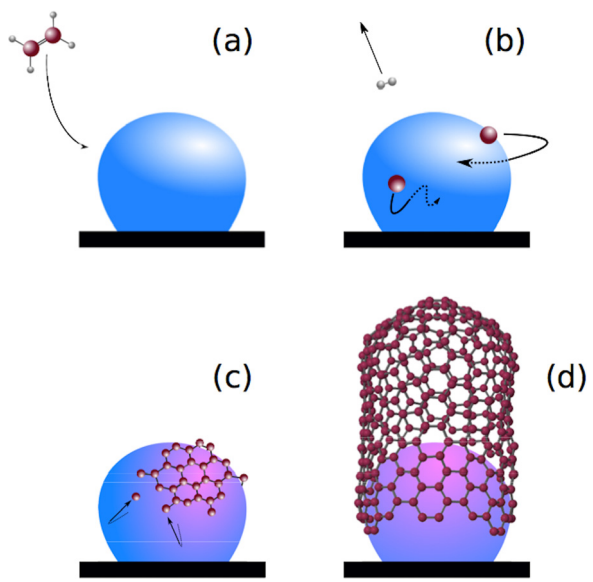

FIG. 5. (Color online) VLS model applied to CNT growth. (a) Adsorption of gas-phase hydrocarbon species on the nanocatalyst particle; (b) catalytic decomposition into carbon atoms and dissolution in the liquid bulk; (c) surface carbon segregation with the formation of a solid precipitate; (d) formation of a solid crystalline structure.

introducing a reinitiation energy barrier for each turn. Note, however, that this model does not address the presence of a catalyst and the nucleation step, but only prolonged growth.

B. Advantages of PECVD growth of CNTs

Very recently, three excellent reviews have appeared in the literature regarding PECVD growth of CNTs.[20,33,42] Therefore, here we shall focus only on the possible advantages of using PECVD over thermal CVD, and the recent advances in generating SWNTs using PECVD.

1. Low temperature growth

It is often mentioned that one of the main advantages of PECVD is the low temperature processing. Correspondingly, various reports have presented low temperature (below ~700 K) growth of MWNTs. However, as pointed out by Meyyappan,[43] many of these reports appear to be somewhat misleading. Indeed, as mentioned earlier, the plasma itself can contribute significantly to heating of the substrate, while in many growth studies the temperature measurement is either done only on the back side of the substrate, or not mentioned at all. The importance of this issue was clearly demonstrated by Teo *et al.*,[44] studying the temperature profile at and in front of the substrate. It was found that the substrate temperature reached values as high as 973 K by plasma heating alone.

One of the few credible low temperature growth claims was reported by Hofmann *et al.*,[39,45,46] using temperature labels as calibration standards. They reported MWNT growth at temperatures as low as 393 K in a dc plasma using an acetylene/ammonia gas mixture at a pressure of 1.5 mbar. An activation energy for the growth rate on nickel was found to be 0.23 eV, which is much lower than the value of 1.2–1.5 eV for thermal CVD. Therefore, this indicates that a different growth mechanism may be operative. It was suggested that in contrast to thermal CVD, the PECVD growth is governed by surface diffusion of carbon atoms to the edge of the growing tube, as mentioned earlier. Furthermore, modeling efforts provided additional evidence for this route, as the energy barrier for C diffusion on an Ni(111) surface was found to be 0.4 eV, close to the growth activation energy.[40]

2. Reactive radicals

PECVD may be advantageous over thermal CVD in the sense that it provides highly reactive, (partially) dehydrogenated species to the catalyst. Thus, whereas a high dehydrogenation barrier must be overcome in thermal CVD on the catalyst surface, this barrier is not, or only partially, present in PECVD growth. This, of course, contributes to the possibility of a low growth temperature.

3. Effect of the plasma on the catalyst

The effect of plasma on the catalyst particles is of crucial importance for the CNT growth itself. For example, it has been demonstrated that the chirality distribution of as-grown SWNTs is influenced by the properties of the nanocatalyst.[47–49] The catalyst particles are of primary importance in CNT growth, and serve at least five goals: (1) adsorption and catalytic decomposition of hydrocarbon source gases; (2) mass transport of carbon by surface or bulk diffusion; (3) nucleation of the tube; (4) providing a structured or nonstructured template for one-dimensional growth; (5) assisting in healing defects in the growing carbon network. The plasma affects the state of the catalyst particles both before the growth, if a plasma pretreatment is used, as well as during the actual growth stage.

a. Effect of plasma pretreatment on the catalyst. Exposing catalyst nanoparticles to a plasma prevents agglomeration of the particles during CNT growth.[50] As this prevents the formation of larger particles, keeping the average diameter small, this provides a route toward the growth of small diameter CNTs, i.e., SWNTs. Furthermore, exposure of the catalyst to the plasma may also aid in restructuring the catalyst.[51] Cantoro *et al.*[52] performed an extensive study on the influence of an NH_3 plasma pretreatment step prior to CNF growth. It was concluded that the plasma pretreatment enhances the growth and density of the CNFs, especially at low temperatures. This net effect can be attributed to various effects. The NH_3 plasma is a source of atomic hydrogen, which may reduce oxides, causing the catalysts to transform into their metallic state. It is this metallic state that is believed to be catalytically active during CNT growth. Likewise, Malesevic *et al.*[16] reported a decrease in catalyst diameter by a factor of 2 and a density increase by a factor of 5 after an H_2 microwave plasma treatment. The reduction of the oxidized metal to the metallic form also was reported.

Besides preventing agglomeration of nanoparticles, restructuring of the catalyst, and the reduction of the oxidized metal to the metallic form, the plasma may also affect the catalyst in the pretreatment step by the action of the electric field. Indeed, the electric field usually leads to ion bombardment, causing erosion of the particles. Furthermore, the plasma also causes ion-induced mobility of the surface atoms. Together with the ion bombardment erosion, this leads to increased roughness. As a result, the plasma pretreatment narrows the particle distribution, so that narrower diameter distributions for nanotubes grown from pretreated substrates can be obtained.

b. Effect of plasma on the catalyst during the growth. Possibly, the plasma may enhance the solubility of C in the catalyst, due to the presence of hydrogen in the plasma.[53,54] Also, the lower CNT growth temperature has an effect on the catalyst during the growth. Indeed, the catalyst may adopt a different surface structure at lower temperature, possibly resulting in epitaxial growth. This has been referred to as one possible route for chirality-selective synthesis.[55–57]

4. Plasma etching

The plasma typically contains etchant species that are not present under thermal CVD conditions. A distinction should

be made between (1) chemical etching, in which a reactive gaseous component reacts with the tube, thereby forming a volatile product, and (2) sputtering, also known as physical etching, in which highly energetic particles physically remove material, without the need of chemically forming volatile products. Thus, an H_2 plasma may chemically etch CNTs during the growth. In Ref. 50, the narrow diameter and chirality distribution was explained by etching of larger diameter structures by the plasma. Zhang *et al.*[58] succeeded in selectively etching SWNTs by a process termed as hydrocarbonation. In this process, the SWNTs react with plasma species, thereby forming a hydrocarbon gas. Interestingly, it was found that while small diameter tubes were etched without selectivity over metallicity while larger diameter tubes remained unaffected, metallic tubes were preferentially etched in the case of medium diameter tubes. This was explained by the more abundant delocalized electronic states in medium diameter tubes. Further, it was found that smaller tubes are more easily etched than larger tubes, due to the higher curvature energy and the higher strain in these SWNTs.[58]

5. Effect of the electric field

Finally, an important contribution to the growth may also result from the electric field. Indeed, the electric field is assumed to be responsible for alignment of CNTs and CNFs during PECVD growth.[39,59–61] Bower *et al.* convincingly demonstrated the alignment of CNTs on flat, tilted, and curved surfaces, attributing the alignment to the electrostatic self-bias at the surface.[60] An example is shown in Fig. 6. More recently, Kato and Hatakeyama,[5] Hatakeyama *et al.*,[33] and Kato *et al.*[62] have shown the growth of vertically aligned freestanding SWNTs in a diffusion plasma. Recent MD simulations demonstrated that the nucleation of SWNTs preferentially occurs at the tip of a nanocatalyst particle, and the growth of the SWNTs subsequently proceeds vertically, by alignment with the electric field.[6] These effects were explained by the small charge separation occurring between the carbon atoms and the metal atoms of the nanoparticle, leading to a competition between the random, thermally driven diffusion of the carbon atoms and the directed, electric field driven migration of the carbon atoms. This effect is illustrated in Fig. 7.

Additionally, a sufficiently strong electric field is usually accompanied by ion bombardment. The importance of ion bombardment was clearly demonstrated by Gohier *et al.*[63,64] These authors found that vertically aligned SWNTs could be obtained when the plasma synthesis time was kept sufficiently short. The growth mechanism was base growth, in which the catalyst particle remained attached to the substrate. Increasing the synthesis time resulted in no observable CNT growth. Increasing the growth time further resulted in the formation of MWNTs by a tip growth mechanism, in which the catalyst particle detached from the surface.

Similarly, Luo *et al.* found a transition from SWNT to MWNT growth due to ion bombardment, especially at low growth rates.[65] These observations are explained by a competition process between catalytic growth of tube structures and C–C bond breaking by ion bombardment. Indeed, when the growth rate is low, the importance of bond breaking events is greater than the bond formation, and growth is inhibited. MWNTs, on the other hand, show higher resistibility against ion bombardment.

Additionally, in the case of tip growth (as is the case of MWNT growth), the catalyst nanoparticle is likely to protect the carbon nanotube against the incoming ions; in contrast to the base growth mechanism (as is the case for SWNT growth). As mentioned earlier, damage due to ion bombardment can be avoided by the use of a remote plasma.[5,66–68]

While many PECVD growth studies yield MWNTs and CNFs as product, it is also possible to generate SWNTs directly with PECVD. The first report on this was by Kato *et al.* in 2003,[62] using zeolites as catalyst support. Since zeolites are nanoporous materials, they keep the catalyst particle size small, allowing only SWNT growth, even at high temperature.

As mentioned earlier, Kato and Hatakeyama[5] also succeeded in growing vertically aligned, freestanding SWNTs in a PECVD setup. The observed alignment was shown to be due to the strong electric field in the plasma sheath. Furthermore, Ghorannevis *et al.*[50,69] succeeded in obtaining narrow chirality distributions using Au as catalyst in their PECVD setup. The addition of a small amount of H_2 was found to be

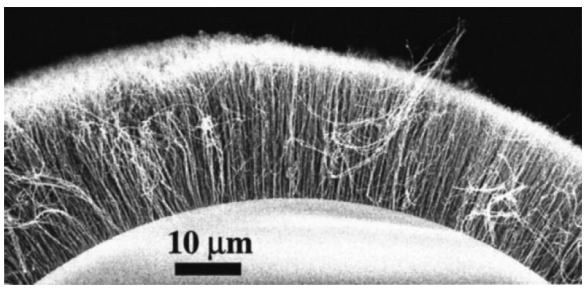

FIG. 6. Plasma induced radial growth of CNTs on the surface of a 125 μm diameter optical fiber. Reprinted with permission from Bower *et al.*, Appl. Phys. Lett. **77**, 830 (2000), American Institute of Physics.

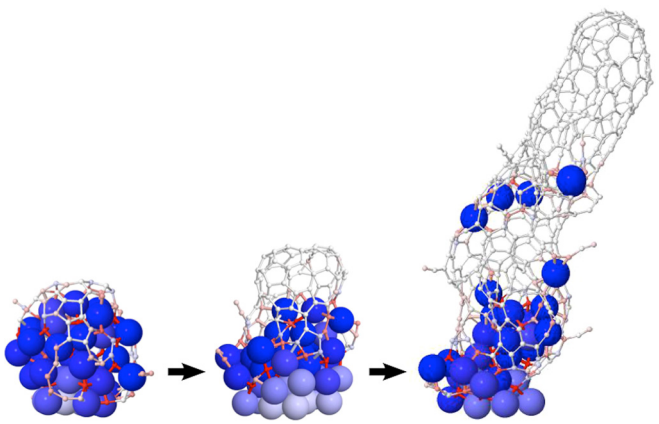

FIG. 7. (Color online) Illustration of the electric field induced alignment during SWNT growth in an MD simulation. Reprinted with permission from Neyts *et al.*, J. Am. Chem. Soc. **134**, 1256 (2012), American Chemical Society.

crucial for obtaining a narrow distribution, with a peak in the (6,5) chirality as determined using photoluminescence excitation. Interestingly, a much broader distribution was found when either using Fe as a catalyst in the PECVD setup, or using Au as the catalyst in a thermal setup. This latter result was explained by the fact that in PECVD, the catalyst particles tend to aggregate less, due to the shorter growth incubation time compared to thermal CVD.

V. MODELING CARBON NANOTUBE GROWTH

PECVD is a very complex process, and hence very difficult to model in all of its details. Rather than trying to model the entire system at once, the process is therefore usually divided into various subsystems, each of which is easier to handle. Thus, various subprocesses can be discerned:

(1) Plasma flow, including mass, species, momentum, and energy transfer, see, e.g., Refs. 70 and 71. These are solved by the mass conservation equation ("continuity equation"), momentum conservation equation, and the energy conservation equation (together these equations are called the Navier–Stokes equations), and the species conservation equation.
(2) Plasma chemistry, including all possible reactions between the constituent particles, see, e.g., Refs. 70–73. These include electron–neutral, ion–neutral, neutral–neutral, ion–ion, and electron–ion reactions.
(3) Plasma–catalyst interactions and the growth of the CNT, see, e.g., Refs. 6 and 74. As is the case in the bulk fluid, the electrons, ions, as well as the neutrals can interact with the catalyst particle. Depending on the phase state of the catalyst particle, the species impinging from the gas phase may be transported either on the surface of the particle or on the surface as well as in the bulk of the particle.

Obviously, these submodels are inherently coupled. Here, we shall mainly focus on the actual growth process, i.e., on the interactions of the plasma species with the catalyst that lead to the formation of the CNT. It should be mentioned, however, that various researchers have also worked on modeling the plasma flow and plasma chemistry for CNT growth.[44,70–73,75–80]

In the following, we will start with the most detailed simulations, operative on the atomic scale, and work toward the more approximate, macroscale-type simulations.

A. Atomistic simulations of CNT growth

Many researchers have worked on the atomistic simulation of CNT growth, using various methods ranging from the quantum mechanical approach to the classical approximation. Until now, however, practically none of these simulations have been specific for PECVD growth, although recently first steps in this direction have been taken.[6] Nevertheless, these simulations provide much information that is relevant for PECVD growth as well. Furthermore, it should also be kept in mind that almost all of these simulations relate to SWNT growth, whereas PECVD very often results in MWNT or CNF growth.

1. Quantum mechanical modeling of CNT growth

The most accurate simulations of CNT growth are based on quantum mechanical methods. To this category belong Car-Parrinello simulations, density functional theory (DFT), tight-binding (TB), and density functional tight-binding (DFTB) calculations. Because of their high computational cost, only very few dynamic simulations have been performed using the so-called Car-Parrinello molecular dynamics (CPMD) technique.[81] Note, however, that none of the simulations mentioned here are specific for PECVD growth, but rather correspond to thermal growth.

Gavillet *et al.*[82] used CPMD to study the metal–carbon segregation process in a mixed Co/C cluster, which was allowed to cool from 2000 to 1500 K. It was found that after 5 ps at 1500 K, about 80% of the C atoms segregated to the surface of the cluster, whereas the Co atoms migrated to the center. The formation of a hexagon connected to two pentagons, and the formation of a network of connected linear chains was considered as the first stage of the nucleation process. While the time scale was very short, this simulation should be considered as a milestone, because it was the first simulation demonstrating the self-organization of carbon on the metal catalytic surface. In the same paper, the authors also described the migration of five carbon atoms on a surface and their incorporation in a preassembled half-fullerene cap, representing an SWNT nucleus. While the simulated incorporating process in the SWNT nucleus corresponds to a base growth mechanism, it could be argued that the existence of a perfect half-fullerene cap on a flat metallic surface is unrealistic.[83]

Raty *et al.*[84] also performed CPMD simulations to study CNT growth. In these simulations, C atoms were placed in various arrangements on the surface of a small Fe cluster. The temperature was thermostatically set to 1200 K. Fast diffusion of the carbon atoms was observed on the surface, initially forming dimers, then short chains, and eventually an sp^2 bonded network. The threefold coordinated carbon atoms were found to be weakly bound to the catalytic surface, allowing cap lift-off. Interestingly, the carbon atoms were not found to dissolve in the metal cluster; it was therefore concluded that supersaturation–segregation processes are not required for CNT growth to occur. This result was also found by Ohta *et al.*,[85] showing that carbon cap nucleation on Fe nanoclusters does not require volume diffusion of carbon into the Fe cluster.

Also, Charlier *et al.*[35] used CPMD simulations, as well as TB-Monte Carlo simulations, in order to investigate the behavior of a single metal atom (Ni or Co) at the top of an open SWNT. These authors found that, in contrast to the scooter mechanism, the metal atom is incorporated in the carbon network. Subsequently, this metal atom allows the accommodation of several newly incoming carbon atoms. This, therefore, corresponds to a closed-end growth mechanism. This process is illustrated in Fig. 8.

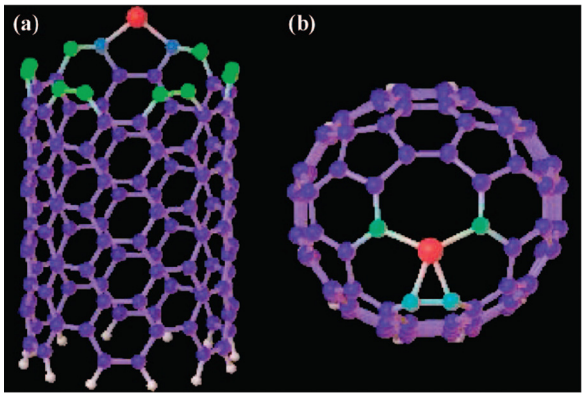

FIG. 8. (Color online) Spontaneous cap closure of a (6,6) SWNT as observed in *ab initio* simulations (Ref. 35), falsifying the scooter growth mechanism. Reprinted with permission from Charlier *et al*., ACS Nano **1**, 202 (2007), American Chemical Society.

A large number of DFTB simulations have been performed (see, e.g., Refs. 85–88) both on Fe and Ni nanoparticles. These simulations focused on the mechanisms and kinetics of cap formation and healing of defects. Growth from both pure metallic and from preformed carbide particles was studied using *ab initio* calculations by Börjesson and Bolton[89] and Page *et al*.[90] They concluded that the growth is possible from both metallic and carbide particles. Page *et al*. also found that SWNT nucleation from Ni_xC_y nanoparticles is more favorable compared to nucleation from Fe_xC_y particles. SWNT nucleation was found to proceed through three distinct steps: the precipitation of carbon from the metal carbide; the formation of a "surface/subsurface" carbide intermediate species; and the formation of a nascent sp^2-hybridized carbon structure supported by the metal catalyst. Related to this carbide formation, Ohta *et al*. demonstrated, also using DFTB, that the formation of a surface carbide is not required for the growth of an SWNT from pure Fe nanoclusters.[85]

Corresponding to the observation of defect healing by the metal by Karoui *et al*.[91] and Neyts *et al*.,[92,93] Page *et al*. also observed defect healing in their DFTB MD growth simulations.[88] This defect healing process occurred via ring isomerization, resulting in the removal of Stone–Wales defects, adatom as well as monovacancy defects.

Nucleation of SWNTs on nickel nanoclusters was also studied by Moors *et al*.[94] and Amara and co-workers[95,96] using a tight-binding Monte Carlo model, focusing on the effect of the chemical potential. In these simulations, it was found that an optimal chemical potential window exists to nucleate graphitic caps that have a curvature compatible with the curvature of the catalyst cluster. The chemical potential should, on the one hand, be large enough to allow a sufficient concentration of carbon atoms on the surface, but, on the other hand, it should not be too large, in order to avoid the formation of amorphous carbon. Karoui *et al*.[91] also extensively discussed the role of the metal catalyst particle. It was found that in addition to catalytic decomposition of the hydrocarbon source gas, it also assists in the nucleation of the initial graphitic islands and assists in defect healing. This is in agreement with classical simulations.[92,93] Karoui *et al*. also found that; in contrast to the *ab initio* data of Fan *et al*.,[97] the interaction between a metallic surface and a graphene flake does not saturate the carbon dangling bonds at the edge of the flake. Rather, the nickel atoms at the surface and in direct contact with the flake are found to be stabilized. Besides dynamical simulations, a number of static *ab initio* calculations also are performed on structures that are considered to be typical for the growing structures or critical in the chain of processes that take place.

Using such static DFT calculations, Lee *et al*. investigated the role of single metal atoms at the edge of SWNTs, concluding that the metal atom must scoot around the open edge of the tube, thereby preventing tube closure.[98] This corresponds to the so-called scooter mechanism as described earlier. This was later contradicted by Andriotis *et al*.[99] and, as mentioned earlier, by Charlier *et al*.[35]

An interesting study was also performed by Zhu *et al*.,[100] focusing on the relationship between the catalyst particle size and the SWNT diameter and chirality. These authors used 0 K DFT calculations and TB simulations at 1000 K, using small Ni clusters as the catalyst. It was found that the graphitic island formation is energetically a costly step, and after its formation the extension of the island into a larger island or an SWNT cap (with various possible chiralities) is spontaneous. Therefore, it was concluded that the island formation determines neither the diameter nor the chirality of the resulting SWNT. Furthermore, it was found that the smallest clusters that allowed for continued growth of (5,5) and (10,0) SWNTs contain about 30–45 atoms, corresponding to an SWNT diameter of 0.84–0.94 nm. The lower limit of the ratio between the diameter of the catalyst cluster and the SWNT was thus found to be about 1.1–1.3, which is in good agreement with the experimental ratios of 1.1–1.6.[101,102]

Also using static DFT calculations, Abild-Pedersen *et al*.[103] studied the interaction of carbon atoms with nickel surfaces. It was found that nickel step edges are the preferred sites for carbon adsorption and act as growth centers for graphene layers. Transport of carbon atoms from these step edges over the nickel surface to the edge of the graphene sheet was found to be surface mediated or subsurface mediated, with overall activation energies of 1.42 and 1.55 eV, respectively, which is in good agreement with the experimentally measured growth energy barriers of about 1.3–1.5 eV.[37,104] The elementary steps for the surface-diffusion mediated process and the associated energy barriers are shown in Fig. 9. Note, however, that the overall energy barrier for bulk diffusion was found to be 2.33 eV. Related to this, Wang and co-workers have very recently demonstrated using DFT calculations that on Ni nanoclusters, the migration of surface carbon atoms into the subsurface region is both thermodynamically and kinetically feasible.[105] These simulations also demonstrated that surface reconstruction of the Ni nanoparticle is an important aspect that should be taken into account in the simulation of CNT growth. Note also that this surface reconstruction is consistent with, e.g., the real-time, *in situ* TEM imaging by Helveg *et al*.[106]

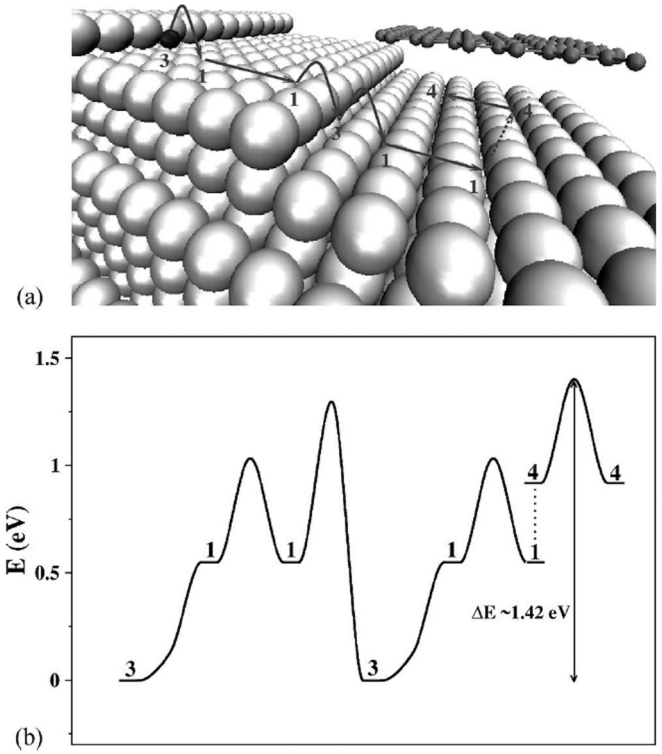

FIG. 9. (a) Elementary steps considered in *ab initio* simulations of C diffusing over an Ni surface; (b) associated energy barriers. Reprinted with permission from Abild-Pedersen *et al.*, Phys. Rev. B **73**, 115419 (2006), American Physical Society.

Reich *et al.*[56] used static DFT calculations to study chirality control of CNTs by epitaxial growth, which is relevant for growth on solid-state catalysts (i.e., at low temperatures, as may be used in PECVD). Two concepts were identified for chirality-selective growth of SWNTs: (1) selectivity must start during nucleation, since a given cap can grow only in an SWNT with a specific chirality; and (2) expitaxial growth favors certain caps and tubes. Also, it was found that the Ni–C bonding favors armchair edges, by a local lattice matching of neighboring C atoms. Chiral selectivity was also investigated by Wang *et al.*[107] Specifically in relation to experimental growth, the authors predicted that the exact concentrations of C atoms and C_2 dimers during the growth should be of crucial importance in chiral-selective growth. Finally, Gomez-Gualdron *et al.*[108] suggest chirality control to be determined by both the kinetics and thermodynamics of the growth process. If the substrate–nanocatalyst interaction is sufficiently strong, the substrate may (1) increase the melting temperature relative to the corresponding floating nanoparticle, and (2) help the nanoparticle to keep its crystallinity. This favors the growth of carbon structures that follow a template determined by the metal surface, and therefore specific nucleation patterns might be favored that are thermodynamically determined. On the other hand, the elevated growth temperatures most likely also allow many other nucleation processes to occur, which therefore widen the chirality distribution. These concepts also naturally lead to the idea of chirality control by lowering the growth temperature, which may be accomplished in PECVD growth.

2. Classical atomistic simulations of CNT growth

As is the case for *ab initio* simulations, classical MD simulations typically consider an idealized thermal CVD growth setup, rather than PECVD. Nevertheless, all of the described studies are also useful for PECVD, although it should be realized that certain key aspects in this respect are missing. Most notably, this concerns the application of electric fields, ion bombardment, chemical etching, and the presence of radicals instead of neutral gas molecules. Recently, some of these effects have been taken into account, as will be mentioned in the following.

Classical MD simulations have been carried out by various authors to gain insight into the growth mechanism (see, e.g., Refs. 57, 92, 93, 109–120). Shibuta and Maruyama[112,113] investigated the nucleation process of SWCNTs, focusing on the effect of pressure and nanocatalyst particle size. These authors found that an optimum rate must exist for the nucleation of the SWNT cap structure, which is determined by the gas-phase density. Furthermore, it was found that when the rate of carbon addition is too high, and significantly exceeds the rate of the annealing process to a hexagonal network, this results in the formation of amorphous carbons covering the catalyst surface. With respect to the cluster size, these authors found that a minimum size is required, and that the SWNT diameter does not necessarily follow the diameter of the particle, which in general is nonspherical.

Zhao *et al.*, on the other hand, found that the most stable caps are formed in their MD simulations when the diameter of the cap coincides or nearly coincides with the diameter of the particle.[110] This also corresponds to experimental observations,[114] and was explained by a reduction of stress at the edges.

The influence of temperature and catalyst particle size on SWNT growth was studied by Ding and co-workers.[109,115–118] Similar to Shibuta and Maruyama,[113] as well as to the above-mentioned *ab initio* simulations of Zhu *et al.*,[100] it was found that a minimum cluster size is needed for SWNT growth. Below this threshold, which in the case of MD simulations is dependent on the exact interatomic potential, the curvature energy is too high so that the SWNT cap cannot nucleate. Above this threshold, the SWNT caps were found to have a diameter similar to the diameter of the nanoparticle. Furthermore, Ding *et al.* also found that a temperature gradient is not required for SWNT growth on small nanoparticles.[117]

As far as the effect of the growth temperature is concerned, it was found that at lower temperatures, diffusion of carbon occurs mostly via surface diffusion, whereas in the case of higher growth temperatures, carbon diffusion occurs through the bulk of the particle.[109] This simulation result corresponds to the conclusion of Hofmann *et al.* based on their experimental growth studies.[46]

Recently, Ribas *et al.* and Burgos *et al.* performed elaborate MD simulations investigating the growth of SWNTs

focusing on the interaction between the metal cluster and the carbon network.[111,119] The authors found that growth either requires a low work of adhesion, a high temperature, or fast carbon diffusion. Larger particles were found to require a smaller work of adhesion in order for cap lift-off to be possible for a given temperature.

Typically, the growth in MD simulations is modeled by the sequential impact of carbon atoms on the nanocatalyst particle. This procedure, however, does not allow for the incorporation of long time scale events, such as diffusion. One possible solution for this issue was presented by Neyts *et al.*,[92] coupling a force biased Monte Carlo model to the MD model. This approach allows longer time scale events to take place in the simulation, albeit at the price of losing time scale information. This approach resulted in the simulated growth of by far less defective structures than typically obtained in pure MD simulations, including both semiconducting SWNTs (Ref. 92) as well as metallic SWNTs,[93] as illustrated in Fig. 10. In fact, these simulations constituted the first simulations in which a specific chirality was obtained.

Very recently, a number of simulations were performed by the same authors in order to take the first steps toward atomistic simulations of the PECVD growth process. In Ref. 6 they presented a classical hybrid MD/MC simulation demonstrating the effect of applying an electric field on the growth of SWNTs.[6] It was found that applying an electric field of sufficient strength results in vertically aligned growth, in agreement with experimental PECVD results (see Fig. 6).[5,60] In Ref. 6 this vertical alignment was explained by the polarization of the C–Ni bonds, on which the electric field acts, pushing the partially negatively charged C atoms toward the tip of the catalyst particle.

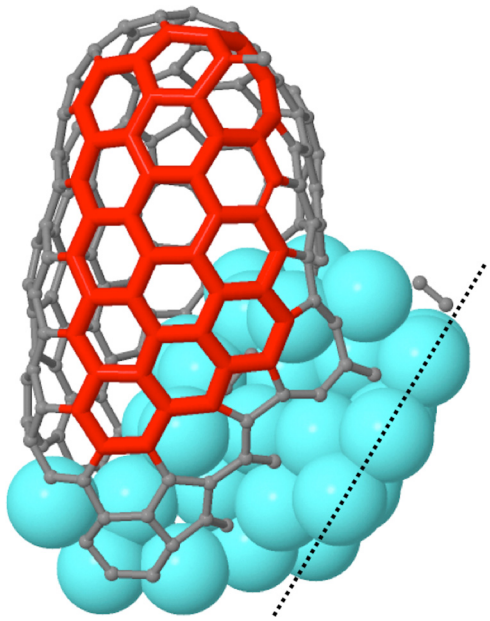

FIG. 10. (Color online) Simulated growth of a (7,7) SWNT in classical MD/MC simulations. The dotted line represents the surface. Reprinted with permission from Neyts *et al.*, J. Am. Chem. Soc. **133**, 17225 (2011), American Chemical Society.

Furthermore, simulations were also carried out to investigate the effect of Ar-ion bombardment on the nucleation of SWNT caps. This indeed is very relevant to PECVD growth, as positive ions from the carrier gas are accelerated toward the substrate by the sheath voltage. It was found that when the ion energy is sufficiently low, i.e., in the order of about 1°eV or lower, the ion bombardment has essentially no effect on the structure of the carbon network. Increasing the ion impact energy to slightly higher values, up to about 25 eV, however, seems to enhance the network formation. This is significant, as in these simulations, no carbon atoms were added that could extend the network.[120] Increasing the ion energy further, to 30 eV and beyond, the destruction of the carbon network is observed, in agreement with the experimental observations of Gohier *et al.*[63]

It can be concluded that many atomistic simulations have already been carried out, providing a lot of information on the atomistic processes that occur during SWNT growth. However, most of these simulations are limited to the CVD case. Only very recently, first efforts to simulate the PECVD process have been undertaken, as explained earlier.

B. Mechanistic models

Besides the atomistic studies on CNT growth described earlier, also various mechanistic models for obtaining a better understanding of the CNT growth process on a larger-than-atomic scale have been developed.[74,121–136] Typically, these models are based on a number of physicochemical processes, such as adsorption and desorption of carbon species at the surface of the metal catalyst particle, surface and bulk diffusion, surface reactions (both on the catalyst surface and the substrate surface), and nanostructure nucleation and growth. While most of these models are applied to CNT growth by CVD, some are also applied for PECVD, and, in general, the principles of the models are the same for both growth techniques. A schematic representation of the various processes included in these mechanistic models is shown in Fig. 11. Table I summarizes different mechanistic growth models recently published in the literature, indicating the reactor type and the processes included in each model.

Mechanistic simulations are particularly attractive because of their simplicity and minor computational effort compared to atomistic simulations. Obviously, however, they lack the atomic scale detail that MD simulations provide. From a simulation point of view, these mechanistic models can be divided into three groups, i.e., kinetic models,[121–128] multiphysics, multiphase integrated models[74,129–132] and kinetic MC models.[133–136]

In a kinetic simulation, all processes included in the model are described either by diffusion coefficients, as is typically done for diffusion processes, or with rate constants, which is the usual approach for chemical reactions. A set of continuity equations is solved as a function of time based on these parameters. This approach allows one to predict the time-dependent growth rate and length of the CNTs, as well as the influence of processing parameters on these quantities.

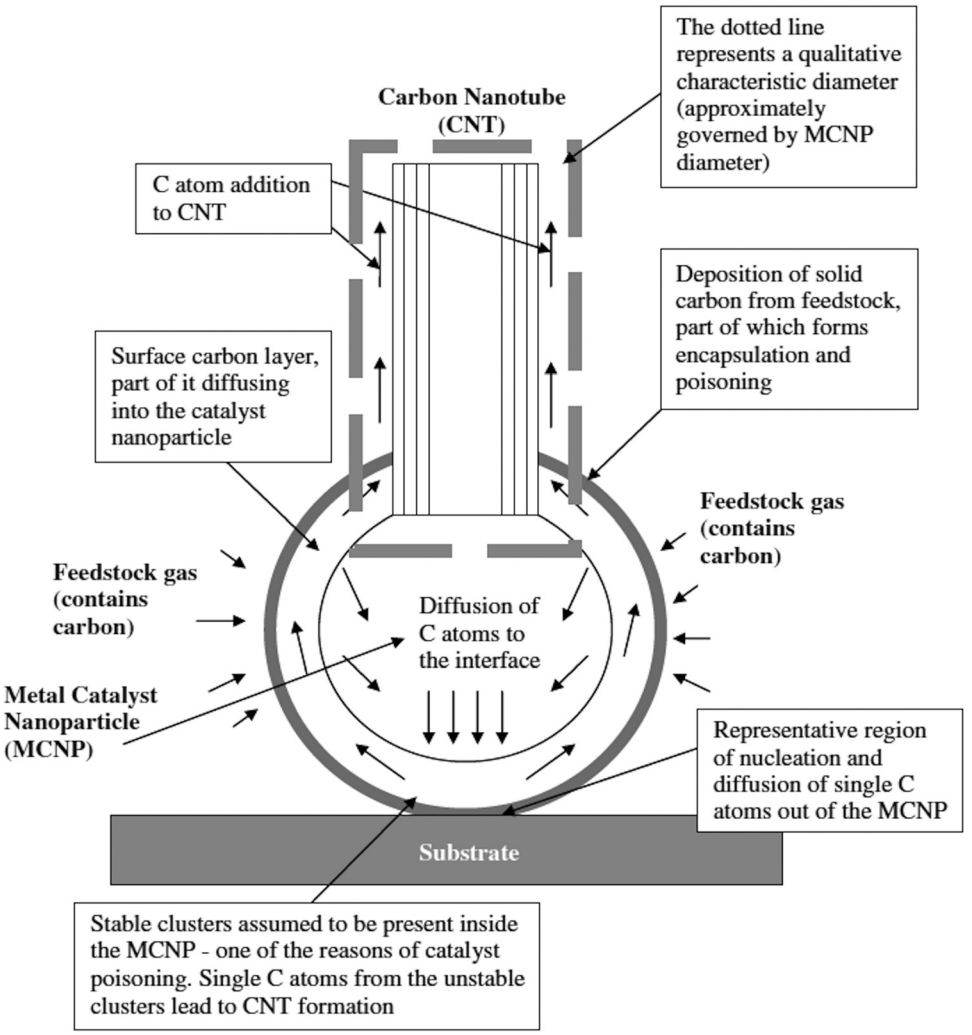

FIG. 11. Typical processes taken into account in mechanistic models of CNT growth. Reprinted with permission from Naha and Puri, J. Phys. D: Appl. Phys. **41**, 065304 (2008), Institute of Physics.

Puretzky and co-workers[121] presented a kinetic model for the CVD-based growth of vertically aligned nanotube arrays (VANTAs) from C_2H_2, based on *in situ* measurements. Besides the above-mentioned processes, the gas-phase decomposition of C_2H_2 and the formation of pyrolysis products in the gas phase and the additional growth of the carbonaceous layer due to these gas-phase pyrolysis products and the catalyst deactivation, were also included. The role of the metal catalyst nanoparticles in VANTA growth, and the optimum size and composition of the catalyst nanoparticles for the fast growth of long and dense VANTAs were analyzed. The simulated results fitted the measurements reasonably well. According to their model, it was found that a change in the oxidation state of

TABLE I. Overview of mechanical models for CNT growth, based on Ref. 137.

	Physicochemical processes				
Reactor	Adsorption and desorption of carbon species	Bulk and surface diffusion	Surface reactions (H abstraction, radical recombination, etc.)	Nanostructure nucleation and growth	Reference
CVD	Yes	Yes	No	Yes	121
CVD	Yes	Yes	Yes	Yes	122,123, 128
CVD	Yes	Yes	No	Yes	124,125
CVD	Yes	No bulk diffusion	Yes	Yes	129
	Yes	No bulk diffusion	Yes	Yes	130–132
PECVD	Yes	Yes	Yes	No nucleation	126,127
PECVD	Yes	Yes	No	Yes	133–136
PECVD	Yes	Yes	Yes	Yes	74

the catalyst nanoparticle, and not the gas-phase pyrolysis products, terminates the growth.

This model was recently further improved by Lee and coworkers[122] by including an additional description for the dependence of the termination length on the size of the catalyst particles and the number of CNT walls. A parametric study showed that the simple kinetic model can successfully predict the kinetics of CNT growth.[122] Although the authors mention that their model is suitable for describing PECVD, important factors such as ion bombardment, hydrocarbon radicals, or the presence of electromagnetic fields were not considered.

A kinetic model of CH_4 decomposition and the subsequent formation of filamentous carbon on supported Co catalysts was presented by Zhang and Smith.[123] The geometry of the catalyst particles was considered and approximated as a slab with height of 2/3 d_p in the model, where d_p denotes the average diameter of a catalyst particle. The model results showed that the Co particle size played an important role in the CH_4 decomposition activity. This model was later improved by Naha *et al.*[124] and applied to the flame synthesis of CNTs and CNFs.

Naha and Puri developed a more detailed kinetic model,[125] based on the models of Puretzky *et al.*,[121] Zhang and Smith,[123] and Naha *et al.*[124] The model included the impingement of C atoms, their adsorption and desorption on the catalyst surface, surface and bulk diffusion, and nucleation and separation of solid C in nanostructured form. The model was validated by comparison to experimental Co-catalyzed CNT growth, and subsequently a parametric study was presented. The model predicts the formation of longer CNTs with increasing temperature and feedstock gas partial pressure, consistent with experiments.[125]

Finally, a phenomenological kinetic model was recently developed by Latorre *et al.*,[128] which included all the relevant steps involved in the CNT growth by catalytic CVD, including carbon source decomposition, nanoparticle surface carburization, carbon diffusion, nucleation, CNT growth, and growth termination by catalyst deactivation or by the effect of sterical hindrance. The model was applied to experimental data, and the values obtained for the kinetic parameters were found to have a realistic physicochemical meaning, in good agreement with the mechanism of CNT formation.[128] Using this model, it was found that the extent of the initial induction period observed during the growth of CNTs can be modulated by modifying the operational conditions, especially the concentration (or molar flux) of the carbon source.

Denysenko and Ostrikov,[126,127] Levchenko and Ostrikov,[133] Levchenko *et al.*,[134,135] and Tam and Ostrikov[136] specifically developed mechanistic models for PECVD of carbon nanostructure growth. The model presented by Denysenko and Ostrikov[126,127] for the PECVD of CNFs is a kinetic model, which accounts for adsorption and desorption of C_2H_2 and H on the catalyst surface, surface and bulk diffusion, incorporation into a graphene sheet, as well as ion- and radical-assisted processes on the catalyst surface that are unique to a plasma environment. It was shown that plasma ions play a key role in the carbon precursor dissociation and surface diffusion, enabling a low temperature growth of carbon nanostructures. In Ref. 127 the plasma heating effects were considered. The authors found that the calculated growth rates were in better agreement with the available experimental data than the results without heating effects.

In order to establish relationships between the fabrication process parameters and the growth conditions for CNTs in (PE)CVD, multiphysics, multiphase integrated models have been developed by several groups.[74,129–132] In these models, all processes of CNT growth are represented by a series of surface reactions. These models bridge the gap between the reactor and molecular length scales. The multiphysics, multiphase models are based on the same principles as the kinetic models, but they are integrated in a reactor model (for CVD) or a plasma model (for PECVD), to obtain self-consistent calculations.

Grujicic *et al.*[129] developed a model to analyze CNT growth by CVD in the presence of Co catalytic particles. The model incorporates coupled boundary-layer laminar-flow hydrodynamics, heat-transfer, gas-phase chemistry, as well as surface chemistry. Optimization of the CNT fabrication process identified the optimum processing parameters that gave rise to a trade-off between a maximization of the overall carbon deposition rate and the amount of carbon deposited as nanotubes.

Lysaght and Chiu reported on a coupled gas phase and surface chemistry model for the CVD of CNTs in a horizontal tube-flow reactor. This model was based on conservation of mass, momentum, and energy equations, in combination with gas-phase and surface chemical reactions.[130,131] The latter are based on adsorption and desorption of the reactive species to and from active sites, hydrogen abstraction from surface bound hydrocarbons, as well as diffusion from the active site toward the nanotube growth edge. The limiting reaction steps for the surface chemistry were identified and the optimum process conditions for efficient CNT production were discussed. Interestingly, it was found that small changes in the number of active sites considered in the model can have large impacts on predicted deposition rates.

Hosseini *et al.* presented a time-dependent multiphysics, multiphase-based model for the CVD-based CNT fabrication process in CH_4/H_2 mixtures.[132] In their model, chemical reactions, fluid dynamics, heat transfer, as well as mass transport phenomena were taken into account. The different CNT synthesis conditions were studied, as a function of temperature and CH_4 and H_2 flow rates. They found that the main role of H_2 gas species during the CNT fabrication process is to reduce the formation of other undesirable forms of carbon structures, such as amorphous carbon.

A multiscale MC/surface diffusion model for the plasma-based growth of carbon nanocone arrays on metal catalyst particles was presented by Levchenko and Ostrikov,[133] Levchenko *et al.*,[134,135] and Tam and Ostrikov.[136] The model comprises three main physical phenomena that play a key role in the nanostructure formation, i.e., (1) diffusion of adsorbed carbon atoms on the substrate surface toward the metal catalyst nanoparticles, (2) dissolution of carbon into

the nanoparticle and eventually carbon saturation of metal catalyst, resulting in nanocone nucleation and growth on top of the catalyst particle, and finally (3) sputtering of the carbon nanocone with impinging carbon ions from the plasma. The model predicts that the plasma parameters can effectively tailor the nanocone array properties and ultimately increase the array quality.

Finally, a very extensive multiphysics, multiphase model was recently presented by Ostrikov and Mehdipour[74] for CNT growth on Au nanoparticles. Their model demonstrates how a constructive interplay between the plasma and the Gibbs–Thomson effect (in this case referred to as the reduction of supersaturation with decreasing size of the growth seed) leads to narrow chirality distributions of thin SWNTs on small nanocatalyst particles at low temperatures and pressures. As such, this model provides essential clues as how to control the chirality distribution in a PECVD growth system.

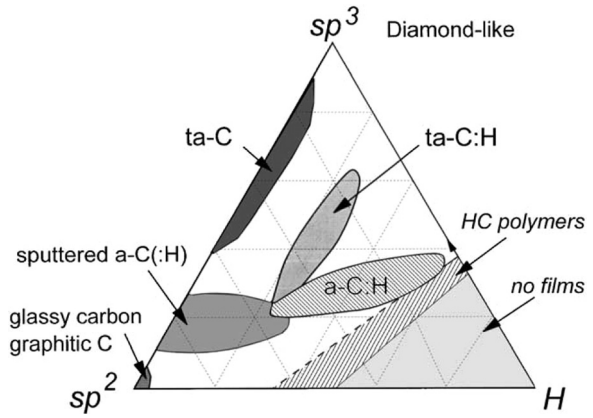

FIG. 12. Ternary phase diagram showing the composition of various amorphous carbons. Reprinted with permission from Robertson, Mater. Sci. Eng. R **37**, 129 (2002), Elsevier.

VI. SHORT OVERVIEW OF MODELING AND SIMULATION RESULTS OF OTHER NANOSTRUCTURED CARBON MATERIALS

A. Graphene

Although its experimental isolation was accomplished only less than 10 years ago, in 2004,[138] graphene is probably the most theoretically studied material. Graphene is popular thanks to its unique properties, including quantum electronic transport, a tunable bandgap, extremely high mobility, or electromechanical modulation.[139–142] Current preparation methods include mechanical exfoliation, ultrahigh vacuum annealing of SiC, CCVD, surface segregation from metallic surfaces, and chemical reduction of graphene oxide.[143–146] Recently, PECVD of graphene (or more often, few-layer graphene) was accomplished. Nevertheless, there are currently no modeling or simulation studies on the PECVD growth of graphene. A few simulation studies have been presented, although these do not relate directly to PECVD. Graphene formation and healing of defects on Ni(111) surfaces was previously simulated by Karoui *et al.*[91] and Amara et al.[95,147] using a grand canonical Monte Carlo tight binding model. Amara *et al.* also studied the interaction between graphitic patches and an Ni(100) surface.[148] Gao *et al.* simulated the formation of small carbon clusters on an Ni(111) surface by DFT, emphasizing the role of pentagons in the graphene island formation.[149]

B. Amorphous carbon

The first amorphous carbon films were grown more than 40 years ago by Aisenberg and Chabot in 1971, using an ion beam system.[150] Often, the exact composition is represented in a ternary phase diagram as illustrated in Fig. 12.[151]

As far as modeling is concerned, most attention in the literature is devoted to the interaction of hydrocarbon molecules and radicals with various surfaces (reaction coefficients),[152–159] and the formation of hard layers from ion sources.[160–164] PECVD growth with emphasis on the chemical growth from reactive radicals; on the other hand, has received much less attention. Very recently, a review on the various PECVD growth studies of amorphous carbon was presented.[165]

Corresponding to *a*-C:H growth in an expanding thermal plasma setup, MD simulations were performed using small hydrocarbon radicals as growth species and an arbitrary H flux of 50% toward the substrate.[166] Under these conditions, a film was formed containing a relatively high fraction of sp^3 carbon of 50%, in reasonable agreement with the experimental value of 67%.[167] The hydrogen fraction was about 45% and the density was around 1.73 g cm^{-3}. The structure of the film was found to be polymeric, also in agreement with the experiment. Therefore, the simulated film was overall in good agreement with the experiment, albeit for an arbitrarily chosen H flux.

Simulations were also performed in which the H flux was varied from 0% to 45%.[168] In agreement with the experiment, nearly no chain terminating CH_3 fragments were found, even for the highest H fluxes. The increasing H fraction in the film triggers a change in hybridization, from *sp* to sp^2 to sp^3. The best quality films were found for an H flux of 10%, resulting in a mass density of about 1.8 g cm^{-3},[168] as shown in Fig. 13. Therefore, these simulations predict that under the specified conditions, the density of the grown films can be controlled to a certain extent by controlling the exact H flux toward the substrate.

When an additional substrate bias is applied, ion bombardment will also affect and contribute to the growth, in addition to the actual growth from low-energy radicals. Therefore, some simulations have also been conducted to investigate the effect of Ar^+ ion bombardment.[169] In these simulations, both the ion energy was varied (from 0.13 to 100 eV), as well as the relative ion flux (from 0.1 to 0.47). The growth species were again chosen based on the experimentally measured hydrocarbon fluxes.

The growth and especially the resulting properties were indeed found to be strongly dependent on the Ar^+ ion energy and relative flux. At low impact energies, the relative ion flux was found to be of little importance, and the differences in structure of the obtained films were a direct consequence

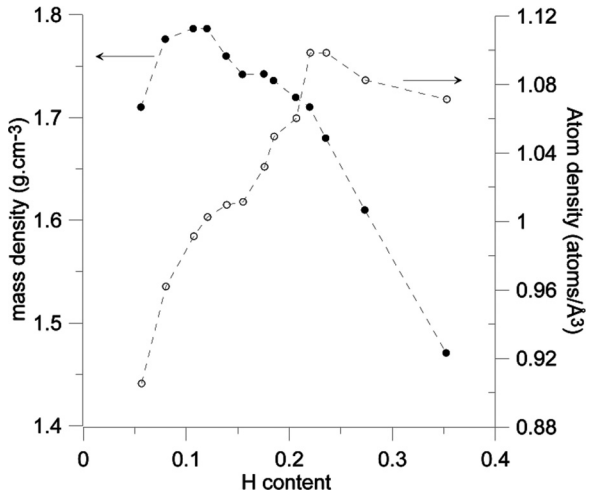

FIG. 13. Effect of adding a controlled H flux during *a*-C:H growth as predicted by MD simulations. These simulations indicate that a densification of the film is possible by adjusting the H content in the film. Reprinted with permission from Neyts *et al*., Appl. Phys. Lett. **88**, 141922 (2006), American Institute of Physics.

of the growth species. As the ion energy was increased, however, the probability of knock-on penetration per ion impact also increases. The total number of knock-on penetrations is further also dependent on the total flux of the ions. The densest films were found at the highest ion energies investigated (100 eV) at the highest relative fluxes (47%). Under these conditions, a mass density of 2.8 g cm^{-3} was obtained.[169] Overall, the results were in agreement with experimental observations, see, e.g., Ref. 151.

C. Metallofullerenes

Metallofullerenes are fullerenes with attached metal atoms—either on the outside of the fullerene cage (termed exohedral metallofullerenes), on the inside (termed endohedral metallofullerenes), or where the metal atom replaces a carbon atom from the cage (termed heterohedral metallofullerenes). Metallofullerenes have been envisaged for use in, e.g., radiotherapy or their use as electronic, optic, and magnetic materials. However, there are almost no simulations available on their formation by a plasma source. Typically, metallofullerenes—either the exohedral, heterohedral, or endohedral variants—are formed by dc electric arc discharges or the laser furnace method. Some metallofullerenes, however, have been experimentally obtained by ion implantation.[170–173]

The possible formation of Ni-metallofullerene was predicted by both classical and *ab initio* MD simulations, by means of ion implantation.[174,175] These simulations predicted that at low Ni-ion impact energies (up to 10 eV), exohedral Ni–C_{60} is formed, at intermediate energies (up to ~40 eV) both the heterohedral Ni–C_{59} and the endohedral Ni@C_{60} metallofullerenes are formed, and at high impact energies (from about 70 eV and above), the C_{60} cage structure was destroyed. This result is illustrated in Fig. 14. Following these simulation predictions, the results were indeed confirmed experimentally.[176]

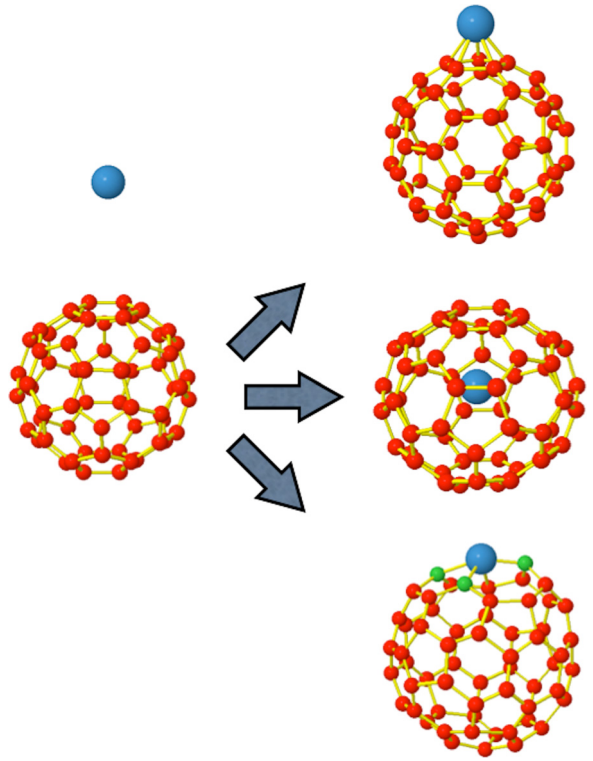

FIG. 14. (Color online) Formation of Ni-metallofullerene, as predicted by both classical and DFT calculations: (a) exohedral; (b) endohedral; (c) heterohedral.

VII. CHALLENGES FOR MODELING AND SIMULATION

As is clear from the above-presented discussions, a lot more experimental work has been carried out regarding PECVD growth of CNTs than computational work, and especially with respect to the atomistic simulations. The ultimate computational study would consist of a self-consistent model comprising the different submodels and the different techniques identified in this review, describing the physics of the growth process from the atomic level up to the macroscopic level. Clearly, however, such a model does not seem feasible on a short term, due to the immense disparity in attainable time and length scales.

More feasible in the near future is to extend the capabilities of the different techniques into the domain of one of the other methods. For instance, current (*ab initio*) TB simulations can handle systems that were previously only accessible by classical MD in both time and length scales. In the following, a number of challenges are identified, which if solved, would bring the computations closer to the experiments.

Currently, all reported quantum mechanical calculations refer to either a highly idealized representation of a particular system (e.g., the diffusion of a single C atom on a perfect metal surface), or to a growth condition that is far away from the actual growth process (e.g., the insertion of carbon atoms in the system instead of hydrocarbon species, or the extremely short growth time scales). Also, when considering growth, the corresponding growth process is typically thermal CVD, rather than PECVD.

Very similar to these approximations in *ab initio* calculations are the approximations made in classical MD simulations. Indeed, also in classical MD simulations, carbon atoms are typically injected into the gas phase and similarly high species fluxes are used in order to observe growth within the accessible time scale. Some progress has been made in this respect, by coupling MC simulations to the MD simulation,[6,92,93] albeit at the price of losing information regarding the elapsed time. Again similar to *ab initio* calculations, classical MD growth simulations typically consider thermal CVD growth, rather than PECVD growth. Also in this respect, some progress has recently been made, by considering the effect of the electric field on the growth[6] as well as the effect of ion bombardment.[120] Certainly, such efforts bring the simulated systems closer to the "real world" growth.

Nevertheless, various challenges remain. First and foremost, the accessible time and length scales remain an important issue. Currently, nanosecond time scales and nanometer length scales can routinely be handled. Real growth experiments, however, typically extend up to seconds or longer, while the length of the tubes before growth termination may reach centimeters. Therefore, techniques that would maintain the atomic detail, but extend into these time and length scale domains, would be highly welcomed. In this respect, it is worth mentioning that a mesoscopic model for continued CNT growth was reported by Elliott *et al.*,[177] although not considering the growth process in atomic detail.

Specific with respect to classical MD simulations is the challenge of constructing reliable and accurate interatomic potentials for describing the interaction of a variety of elements with carbon. Indeed, not only the elements of which the nanoparticle consist must be considered (e.g., Fe, Co, Ni, Si and O for SiO_2 Au, etc.), but also other elements present in the system such as Ar, He, H (e.g., in hydrocarbons), N (in N_2), or O (e.g., in H_2O) should be taken into account. One good candidate to resolve this challenge is the so-called ReaxFF potential, for which tens of elements and their compounds have already been parameterized.[178]

The second challenge is to take into account factors that are experimentally known to be of importance, but have never been considered practically, until now, in any simulation. Such factors, which are relevant both for thermal and for plasma enhanced growth, include the influence of the surface and further substrate layers, the actual growth precursor (e.g., methane, acetylene,.etc.), the role of the carrier gas or dilutent, the possible multielement structure of the catalyst, and so on.

The third crucial challenge is to address the PECVD-specific factors. These include (but are not limited to) the influence of electromagnetic fields on the growth, ion bombardment, growth from hydrocarbon radicals (instead of from carbon atoms), and the influence of etchant species.

With respect to the mechanistic modeling, the most important challenge is to rely on data that is accurate. That is, mechanistic models typically depend on a large number of parameters which are used in the formulas describing the various physical and chemical processes considered in the model. The ultimate results that come from these models are therefore determined by the exact balance of all these processes and hence of these parameters. Therefore, at least a number of sensitivity studies need to be carried out to assess to what extent each process depends on the exact value of the parameters used. For these models, it is therefore of the utmost importance to collect as much reliable data as possible from which these parameters can be determined.

Finally, bridging the gap between computations and experiments can also be facilitated by dedicated experiments providing data that can be used, on the one hand, as input for the simulations (such as accurate data on radical densities, ion fluxes and energies,.etc,.), and, on the other hand, experiments that consider the limitations of the computations. As such, experimental growth studies using nanocatalyst particles as small as possible, consisting of only one element, with very high growth rates, from simple gases and without multilayered substrates would be warmly welcomed by the simulation community.

ACKNOWLEDGMENTS

The author gratefully acknowledges insightful discussions with A. Bogaerts from the University of Antwerp and K. Ostrikov from CSIRO, Sydney.

[1]A. Bogaerts, E. Neyts, R. Gijbels, and J. van der Mullen, Spectrochim. Acta, Part B **57**, 609 (2002).
[2]A. Grill, *Cold Plasma in Materials Fabrication: From Fundamentals to Applications* (IEEE, New York, 1994).
[3]K. Ostrikov, *Plasma Nanoscience* (Wiley-VCH, Weinheim, 2008).
[4]B. Chapman, *Glow Discharge Processes* (Wiley, New York, 1980).
[5]T. Kato and R. Hatakeyama, Chem. Vap. Deposition **12**, 345 (2006).
[6]E. C. Neyts, A. C. T. van Duin, and A. Bogaerts, J. Am. Chem. Soc. **134**, 1256 (2012).
[7]M. A. Lieberman and A. J. Lichtenberg, *Principles of Plasma Discharges and Materials Processing* (Wiley, New York, 1994).
[8]L. Delzeit, I. McAninch, B. A. Cruden, D. Hash, B. Chen, J. Han, and M. Meyyappan, J. Appl. Phys. **91**, 6027 (2002).
[9]K. Matthews, B. Cruden, B. Chen, M. Meyyappan, and L. Delzeit, J. Nanosci. Nanotechnol. **2**, 475 (2002).
[10]S. Xu, K. N. Ostrikov, Y. Li, E. L. Tsakadze, and I. R. Jones, Phys. Plasmas **8**, 2549 (2001).
[11]T. Yuji and Y. M. Sung, IEEE Trans. Plasma Sci. **35**, 1027 (2007).
[12]S. H. Tsai, C. W. Chao, C. L. Lee, and H. C. Shih, Appl. Phys. Lett. **74**, 3462 (1999).
[13]Y. C. Choi, Y. H. Lee, B. S. Lee, G. Park, W. B. Choi, N. S. Lee, and J. M. Kim, J. Vac. Sci. Technol. A **18**, 1864 (2000).
[14]J. Y. Lee and B. S. Lee, Thin Solid Films **418**, 85 (2002).
[15]S. K. Srivastava, A. K. Shukla, V. D. Vankar, and V. Kumar, Thin Solid Films **492**, 124 (2005).
[16]A. Malesevic, H. Chen, T. Hauffman, A. Vanhulsel, H. Terryn, and C. Van Haesendonck, Nanotechnology **18**, 455602 (2007).
[17]L. Qu, F. Du, and L. Dai, Nano Lett. **8**, 2682 (2008).
[18]E. J. Bae, Y.-S. Min, D. Kang, J.-H. Ko, and W. Part, Chem. Mater. **17**, 5141 (2005).
[19]T. Nozaki, S. Yoshida, T. Karatsu, and K. Okazaki, J. Phys. D: Appl. Phys. **44**, 174007 (2011).
[20]M. Meyyappan, J. Phys. D: Appl. Phys. **44**, 174002 (2011).
[21]S. Iijima, Nature (London) **354**, 56 (1991).
[22]S. Iijima and T. Ichihashi, Nature (London) **363**, 603 (1993).
[23]D. S. Bethune, C. H. Riang, M. S. de Vries, G. Gorman, R. Savoy, J. Vazquez, and R. Beyers, Nature (London) **363**, 605 (1993).
[24]P. M. Ajayan, J. M. Lambert, P. Bemier, L. Barbedette, C. Colliex, and J. M. Planeix, Chem. Phys. Lett. **215**, 509 (1993).
[25]M. S. Dresselhaus and Ph. Avouris, *Carbon Nanotubes: Synthesis, Structure, Properties and Applications*, edited by M. S. Dresselhaus, G. Dresselhaus, and Ph. Avouris (Springer, Heidelberg, 2001), pp. 3–6.

[26]M.-F. Yu, O. Lourie, M. J. Dyer, K. Moloni, T. F. Kelly, and R. S. Ruoff, Science **287**, 637 (2000).
[27]B. G. Demczyk, Y. M. Wang, J. Cumings, M. Hetman, W. Han, A. Zettl, and R. O. Ritchie, Mater. Sci. Eng., A **334**, 173 (2002).
[28]M. Popov, M. Kyotani, R. J. Nemanich, and Y. Koga, Phys. Rev. B **65**, 033408 (2002).
[29]S. Hong and S. Myung, Nat. Nanotechnol. **2**, 207 (2007).
[30]K. Mizuno, J. Ishii, H. Kishida, Y. Hayamizu, S. Yasuda, D. N. Futaba, M. Yumura, and K. Hata, Proc. Natl. Acad. Sci. U.S.A. **106**, 6044 (2009).
[31]E. Pop, D. Mann, Q. Wang, K. Goodson, and H. Dai, Nano Lett. **6**, 96 (2006).
[32]R. H. Baughman, A. A. Zahkidov, and W. A. de Heer, Science **297**, 787 (2002).
[33]R. Hatakeyama, T. Kaneko, T. Kato, and Y. F. Li, J. Phys. D: Appl. Phys. **44**, 174004 (2011).
[34]A. Thess *et al.*, Science **273**, 483 (1996).
[35]J.-C. Charlier, H. Amara, and Ph. Lambin, ACS Nano **1**, 202 (2007).
[36]R. S. Wagner and W. C. Ellis, Appl. Phys. Lett. **4**, 89 (1964).
[37]R. T. K. Baker, M. A. Barber, P. S. Harris, and R. J. Waite, J. Catal. **26**, 51 (1972).
[38]A. J. Page, K. R. S. Chandrakumar, S. Irle, and K. Morokuma, J. Am. Chem. Soc. **133**, 621 (2011).
[39]S. Hofmann, C. Ducati, J. Robertson, and B. Kleinsorge, Appl. Phys. Lett. **83**, 135 (2003).
[40]S. Hofmann, G. Csanyi, A. C. Ferrari, M. C. Payne, and J. Robertson, Phys. Rev. Lett. **95**, 036101 (2005).
[41]F. Ding, A. R. Harutyunyan, and B. I. Yakobson, Proc. Natl. Acad. Sci. U.S.A. **106**, 2506 (2009).
[42]R. M. Sankaran, J. Phys. D: Appl. Phys. **44**, 174005 (2011).
[43]M. Meyyappan, J. Phys. D: Appl. Phys. **42**, 213001 (2009).
[44]K. B. K. Teo *et al.*, Nano Lett. **4**, 921 (2004).
[45]S. Hofmann, C. Ducati, B. Kleinsorge, and J. Robertson, Appl. Phys. Lett. **83**, 4661 (2003).
[46]S. Hofmann, B. Kleinsorge, C. Ducati, A. C. Ferrari, and J. Robertson, Diamond Relat. Mater. **13**, 1171 (2004).
[47]S. M. Bachilo, L. Balzano, J. E. Herrera, F. Pompeo, D. E. Resasco, and R. B. Weisman, J. Am. Chem. Soc. **125**, 11186 (2003).
[48]Y. H. Miyauchi, S. H. Chiashi, Y. Murakami, Y. Hayashida, and S. Maruyama, Chem. Phys. Lett. **387**, 198 (2004).
[49]X. L. Li, X. M. Tu, S. Zaric, K. Welsher, W. S. Seo, W. Zhao, and H. J. Dai, J. Am. Chem. Soc. **129**, 15770 (2007).
[50]Z. Ghorannevis, T. Kato, T. Kaneko, and R. Hatakeyama, J. Am. Chem. Soc. **132**, 9570 (2010).
[51]M. Cantoro *et al.*, Nano Lett. **6**, 1107 (2006).
[52]M. Cantoro *et al.*, J. Appl. Phys. **105**, 064304 (2009).
[53]C. Ducati, I. Alexandrou, M. Chhowalla, J. Robertson, and G. A. J. Amaratunga, J. Appl. Phys. **95**, 6387 (2004).
[54]A. Badzian and T. Badzian, Diamond Relat. Mater. **5**, 93 (1996).
[55]W.-H. Chiang and R. M. Sankaran, Nature Mater. **8**, 882 (2009).
[56]S. Reich, L. Li, and J. Robertson, Chem. Phys. Lett. **421**, 469 (2006).
[57]Y. Shibuta, Diamond Relat. Mater. **20**, 334 (2011).
[58]G. Zhang *et al.*, Science **314**, 974 (2006).
[59]M. Chhowalla, K. B. K. Teo, C. Ducati, N. L. Rupesinghe, G. A. J. Amaratunga, A. C. Ferrari, D. Roy, J. Robertson, and W. I. Milne, J. Appl. Phys. **90**, 5308 (2001).
[60]C. Bower, W. Zhu, S. Jin, and O. Zhou, Appl. Phys. Lett. **77**, 830 (2000).
[61]J.-M. Ting and K.-H. Liao, Chem. Phys. Lett. **396**, 469 (2004).
[62]T. Kato, G.-H. Jeong, T. Hirata, R. Hatakeyama, K. Tohji, and K. Motomiya, Chem. Phys. Lett. **381**, 422 (2003).
[63]A. Gohier, T. M. Minea, A. M. Djouadi, A. Granier, and M. Dubosc, Chem. Phys. Lett. **421**, 242 (2006).
[64]A. Gohier, T. M. Minea, S. Point, J.-Y. Mevellec, J. Jimenez, M. A. Djouadi, and A. Granier, Diamond Relat. Mater. **18**, 61 (2009).
[65]Z. Luo, S. Lim, Y. You, J. Miao, H. Gong, J. Zhang, S. Wang, J. Lin, and Z. Shen, Nanotechnology **19**, 255607 (2008).
[66]Y. Y. Wang, S. Gupta, and R. J. Nemanich, Appl. Phys. Lett. **85**, 2601 (2004).
[67]Y. Li *et al.*, Nano Lett. **4**, 317 (2004).
[68]Y. S. Min, E. J. Bae, B. S. Oh, D. Kang, and W. Park, J. Am. Chem. Soc. **127**, 12498 (2005).
[69]Z. Ghorannevis, T. Kato, T. Kaneko, and R. Hatakeyama, Jpn. J. Appl. Phys. **49**, 02BA01 (2010).
[70]M. Mao and A. Bogaerts, J. Phys. D: Appl. Phys. **43**, 315203 (2010).
[71]M. Mao and A. Bogaerts, J. Phys. D: Appl. Phys. **43**, 205201 (2010).
[72]D. Hash, D. Bose, T. R. Govindan, and M. Meyyappan, J. Appl. Phys. **93**, 6284 (2003).
[73]A. Okita, Y. Suda, A. Ozeki, H. Sugawara, Y. Sakai, A. Oda, and J. Nakamura, J. Appl. Phys. **99**, 014302 (2006).
[74]K. Ostrikov and H. Mehdipour, ACS Nano **5**, 8372 (2011).
[75]I. B. Denysenko, S. Xu, J. D. Long, P. P. Rutkevych, N. A. Azarenkov, and K. Ostrikov, J. Appl. Phys. **95**, 2713 (2004).
[76]D. B. Hash and M. Meyyappan, J. Appl. Phys. **93**, 750 (2003).
[77]I. Levchenko, K. Ostrikov, M. Keidar, and U. Cvelbar, J. Phys. D: Appl. Phys. **41**, 132004 (2008).
[78]M. S. Bell, K. B. K. Teo, and W. I. Milne, J. Phys. D: Appl. Phys. **40**, 2285 (2007).
[79]M. Grujicic, G. Cao, and B. Gersten, J. Mater. Sci. **38**, 1819 (2003).
[80]D. B. Hash, M. S. Bell, K. B. K. Teo, B. A. Cruden, W. I. Milne, and M. Meyyappan, Nanotechnology **16**, 925 (2005).
[81]R. Car and M. Parrinello, Phys. Rev. Lett. **55**, 2471 (1985).
[82]J. Gavillet, A. Loiseau, C. Journet, F. Willaime, F. Ducastelle, and J.-C. Charlier, Phys. Rev. Lett. **87**, 275504 (2001).
[83]S. Irle, Y. Ohta, Y. Okamote, A. J. Page, Y. Wang, and K. Morokuma, Nano Res. **2**, 755 (2009).
[84]J.-Y. Raty, F. Gygi, and G. Galli, Phys. Rev. Lett. **95**, 096103 (2005).
[85]Y. Ohta, Y. Okamoto, A. J. Page, S. Irle, and K. Morokuma, ACS Nano **3**, 3413 (2009).
[86]A. J. Page, Y. Ohta, S. Irle, and K. Morokuma, Acc. Chem. Res. **43**, 1375 (2010).
[87]Y. Ohta, Y. Okamoto, S. Irle, and K. Morokuma, ACS Nano **2**, 1437 (2008).
[88]A. J. Page, Y. Ohta, Y. Okamoto, S. Irle, and K. Morokuma, J. Phys. Chem. C **113**, 20198 (2009).
[89]A. Borjesson and K. Bolton, J. Phys. Chem. C **114**, 18045 (2010).
[90]A. J. Page, H. Yamane, Y. Ohta, S. Irle, and K. Morokuma, J. Am. Chem. Soc. **132**, 15699 (2010).
[91]S. Karoui, H. Amara, C. Bichara, and F. Ducastelle, ACS Nano **4**, 6114 (2010).
[92]E. C. Neyts, Y. Shibuta, A. C. T. van Duin, and A. Bogaerts, ACS Nano **4**, 6665 (2010).
[93]E. C. Neyts, A. C. T. van Duin, and A. Bogaerts, J. Am. Chem. Soc. **133**, 17225 (2011).
[94]M. Moors, H. Amara, T. Visart de Bocarmé, C. Bichara, F. Ducastelle, N. Kruse, and J.-C. Charlier, ACS Nano **3**, 511 (2009).
[95]H. Amara, J.-M. Roussel, C. Bichara, J.-P. Gaspard, and F. Ducastelle, Phys. Rev. B **79**, 014109 (2009).
[96]H. Amara, C. Bichara, and F. Ducastelle, Phys. Rev. Lett. **100**, 056105 (2008).
[97]X. Fan, R. Buczko, A. A. Puretzky, D. B. Geohegan, J. Y. Howe, S. T. Pantelides, and S. J. Pennycook, Phys. Rev. Lett. **90**, 145501 (2003).
[98]Y. H. Lee, S. G. Kim, and D. Tomanek, Phys. Rev. Lett. **78**, 2393 (1998).
[99]A. N. Andriotis, M. Menon, and G. Froudakis, Phys. Rev. Lett. **85**, 3193 (2000).
[100]W. Zhu, A. Börjesson, and K. Bolton, Carbon **48**, 470 (2010).
[101]D. Kondo, S. Sato, and Y. Awano, Chem. Phys. Lett. **422**, 481 (2006).
[102]A. G. Nasibulin, P. V. Pikhitsa, H. Jiang, and E. Kauppinen, Carbon **43**, 2251 (2005).
[103]F. Abild-Pedersen, J. K. Nørskov, J. R. Rostrup-Nielsen, J. Sehested, and S. Helveg, Phys. Rev. B **73**, 115419 (2006).
[104]D. L. Trimm, Catal. Rev. - Sci. Eng. **16**, 155 (1977).
[105]Q. Wang, K. H. Lim, S.-W. Yang, Y. Yang, and Y. Chen, Theor. Chem. Acc. **128**, 17 (2011).
[106]S. Helveg, C. Lopez-Cartes, J. Sehested, P. L. Hansen, B. S. Clausen, J. R. Rostrup-Nielsen, F. Abild-Pedersen, and J. Nørskov, Nature (London) **427**, 426 (2004).
[107]Q. Wang, M.-F. Ng, S.-W. Yang, Y. Yang, and Y. Chen, ACS Nano **4**, 939 (2010).
[108]D. A. Gomez-Gualdron, J. Zhao, and P. B. Balbuena, J. Chem. Phys.**134**, 014705 (2011).
[109]F. Ding, A. Rosén, and K. Bolton, Carbon **43**, 2215 (2005).
[110]J. Zhao, A. Martinez-Limia, and P. B. Balbuena, Nanotechnology **16**, S575 (2005).
[111]M. A. Ribas, F. Ding, P. B. Balbuena, and B. I. Yakobson, J. Chem. Phys. **131**, 224501 (2009).
[112]Y. Shibuta and S. Maruyama, Physica B **323**, 187 (2002).
[113]Y. Shibuta and S. Maruyama, Chem. Phys. Lett. **382**, 381 (2003).

[114]W. E. Alvarez, F. Pompeo, J. E. Herrera, L. Balzano, and D. E. Resasco, Chem. Mater. **14**, 1853 (2002).
[115]F. Ding, A. Rosén, and K. Bolton, J. Chem. Phys. **121**, 2775 (2004).
[116]F. Ding, A. Rosén, and K. Bolton, Chem. Phys. Lett. **393**, 309 (2004).
[117]F. Ding, K. Bolton, and A. Rosén, Appl. Surf. Sci. **252**, 5254 (2006).
[118]F. Ding, K. Bolton, and A. Rosén, Comput. Mater. Sci. **35**, 243 (2006).
[119]J. C. Burgos, H. Reyna, B. I. Yakobson, and P. B. Balbuena, J. Phys. Chem. C **114**, 6952 (2010).
[120]E. C. Neyts, A. C. T. van Duin, and A. Bogaerts, "Enhanced carbon nanotube nucleation by low energy ion bombardment," (unpublished).
[121]A. A. Puretzky, D. B. Geohegan, S. Jesse, I. N. Ivanov, and G. Eres, Appl. Phys. A **81**, 223 (2005).
[122]D. H. Lee, S. O. Kim, and W. J. Lee, J. Phys. Chem. C **114**, 3454 (2010).
[123]Y. Zhang and K. J. Smith, J. Catal. **231**, 354 (2005).
[124]S. Naha, S. Sen, A. K. De, and I. K. Puri, Proc. Combust. Inst. **31**, 1821 (2007).
[125]S. Naha and I. K. Puri, J. Phys. D: Appl. Phys. **41**, 065304 (2008).
[126]I. Denysenko and K. Ostrikov, Appl. Phys. Lett. **90**, 251501 (2007).
[127]I. Denysenko and K. Ostrikov, J. Phys. D: Appl. Phys. **42**, 015208 (2009).
[128]N. Latorre, E. Romeo, F. Cazaña, T. Ubieto, C. Royo, J. I. Villacampa, and A. Monzón, J. Phys. Chem. C **114**, 4773 (2010).
[129]M. Grujicic, G. Cao, and B. Gersten, Appl. Surf. Sci. **199**, 90 (2002).
[130]A. C. Lysaght and W. K. S. Chiu, Nanotechnology **19**, 165607 (2008).
[131]A. C. Lysaght and W. K. S. Chiu, Nanotechnology **20**, 115605 (2009).
[132]M. R. Hosseini, N. Jalili, and D. A. Bruce, AIChE J. **55**, 3152 (2009).
[133]I. Levchenko and K. Ostrikov, Appl. Phys. Lett. **92**, 063108 (2008).
[134]I. Levchenko, K. Ostrikov, D. Mariotti, and A. B. Murphy, J. Appl. Phys. **104**, 073308 (2008).
[135]I. Levchenko, K. Ostrikov, J. Khachan, and S. V. Vladimirov, Phys. Plasmas **15**, 103501 (2008).
[136]E. Tam and K. Ostrikov, Nanotechnology **20**, 375603 (2009).
[137]A. Bogaerts, M. Eckert, M. Mao, and E. Neyts, J. Phys. D: Appl. Phys. **44**, 174030 (2011).
[138]K. S. Novoselov, A. K. Geim, S. V. Morozov, D. Jiang, Y. Zhang, S. V. Dubonos, I. V. Grigorieva, and A. A. Firsov, Science **306**, 666 (2004).
[139]Y. Zhang, Y. W. Tan, H. L. Stormer, and P. Kim, Nature (London) **438**, 201 (2005).
[140]M. Y. Han, B. Oezyilmaz, Y. Zhang, and P. Kim, Phys. Rev. Lett. **98**, 206805 (2007).
[141]K. I. Bolotin, K. J. Sikes, Z. Jiang, M. Klima, G. Fudenberg, J. Hone, P. Kim, and H. L. Stormer, Solid State Commun. **146**, 351 (2008).
[142]J. S. Bunch, A. M. van der Zande, S. S. Verbridge, I. W. Frank, D. M. Tanenbaum, J. M. Parpia, H. G. Craighead, and P. L. McEuen, Science **315**, 490 (2008).
[143]K. S. Kim *et al.*, Nature (London) **457**, 706 (2009).
[144]X. Li, G. Y. Zhang, X. D. Bai, X. M. Sun, X. R. Wang, E. Wang, and H. J. Dai, Nat. Nanotechnol. **3**, 538 (2008).
[145]G. Eda, G. Fanchini, and M. Chhowalla, Nat. Nanotechnol. **3**, 270 (2008).
[146]M. Xu, D. Fujita, K. Sagisaka, E. Watanabe, and N. Hanagata, ACS Nano **5**, 1522 (2011).
[147]H. Amara, C. Bichara, and F. Ducastelle, Phys. Rev. B **73**, 113404 (2006).
[148]H. Amara, C. Bichara, and F. Ducastelle, Surf. Sci. **602**, 77 (2008).
[149]J. Gao, Q. Yuan, H. Hu, J. Zhao, and F. Ding, J. Phys. Chem. C **115**, 17695 (2011).
[150]S. Aisenberg and R. Chabot, J. Appl. Phys. **42**, 2953 (1971).
[151]J. Robertson, Mater. Sci. Eng. R **37**, 129 (2002).
[152]E. D. de Rooij, A. W. Kleyn, and W. J. Goedheer, Phys. Chem. Chem. Phys. **12**, 14067 (2010).
[153]P. Träskelin, E. Salonen, A. V. Krasheninnikov, and J. Keinonen, J. Appl. Phys. **93**, 1826 (2003).
[154]A. R. Sharma, R. Schneider, U. Toussaint, and K. Nordlund, J. Nucl. Mater. **363**, 1283 (2007).
[155]P. Träskelin, O. Saresoja, and K. Nordlund, J. Nucl. Mater. **375**, 270 (2008).
[156]E. Neyts, M. Tacq, and A. Bogaerts, Diamond Relat. Mater. **15**, 1663 (2006).
[157]E. Neyts, A. Bogaerts, and M. C. M. van de Sanden, J. Appl. Phys. **99**, 014902 (2006).
[158]E. Neyts, A. Bogaerts, R. Gijbels, J. Benedikt, and M. C. M. van de Sanden, Nucl. Instrum. Methods Phys. Res. B **228**, 315 (2005).
[159]M. Eckert, E. Neyts, and A. Bogaerts, J. Phys. D: Appl. Phys. **41**, 032006 (2008).
[160]H. U. Jäger and A. Belov, Phys. Rev. B **68**, 1 (2003).
[161]A. Belov and H. U. Jäger, Comput. Mater. Sci. **24**, 16 (2003).
[162]N. Marks, J. Phys.: Condens. Mater. **14**, 2901 (2002).
[163]W. L. Quan, H. X. Li, F. Zhao, L. Ji, W. Du, H. D. Zhou, and J. M. Chen, Phys. Lett. A **374**, 2150 (2010).
[164]W. L. Quan, H. X. Li, F. Zhao, L. Ji, W. Du, H. D. Zhou, and J. M. Chen, Chin. Phys. Lett. **27**, 088102 (2010).
[165]E. Neyts, M. Mao, M. Eckert, and A. Bogaerts, *Plasma Processing of Nanomaterials*, edited by R. M. Sankaran (CRC Press, Boca Raton, FL, 2012), pp. 245–290.
[166]E. Neyts, A. Bogaerts, R. Gijbels, J. Benedikt, and M. C. M. van de Sanden, Diamond Relat. Mater. **13**, 1873 (2004).
[167]A.-L. Hamon, J. Verbeeck, D. Schryvers, J. Benedikt, and R. M. C. M. van de Sanden, J. Mater. Chem. **14**, 2030 (2004).
[168]E. Neyts, A. Bogaerts, and M. C. M. van de Sanden, Appl. Phys. Lett. **88**, 141922 (2006).
[169]E. Neyts, M. Eckert, and A. Bogaerts, Chem. Vap. Deposition **13**, 312 (2007).
[170]Z. Wan, J. F. Christian, and S. L. Anderson, Phys. Rev. Lett. **69**, 1352 (1992).
[171]Y. Basir and S. L. Anderson, J. Chem. Phys. **107**, 8370 (1997).
[172]S. Watanabe, N. S. Ishioka, T. Sekine, A. Osa, M. Koizumi, H. Shimomura, K. Yoshikawa, and H. Muramatsu, J. Radioanal. Nucl. Chem. **255**, 495 (2003).
[173]A. Kaplan, A. Bekkerman, B. Tsipinyuk, and E. J. Kolodney, J. Chem. Phys. **117**, 3484 (2002).
[174]E. Neyts and A. Bogaerts, Carbon **47**, 1028 (2009).
[175]E. Neyts, A. Maeyens, G. Pourtois, and A. Bogaerts, Carbon **49**, 1013 (2011).
[176]T. Umakoshi, H. Ishida, T. Kaneko, and R. Hatakeyama, Plasma Fusion Res.: Rapid Commun. **6**, 1206015 (2011).
[177]J. A. Elliott, M. Hamm, and Y. Shibuta, J. Chem. Phys. **130**, 034704 (2009).
[178]A. C. T. van Duin, S. Dasgupta, F. Lorant, and W. A. Goddard, III, J. Phys. Chem. A **105**, 9396 (2001).